Characteristics of Barotropic-Baroclinic Interactions during the Formation of Blocking Events in the Pacific Region

Yasushi WATARAI

Doctoral Program in Geoscience, University of Tsukuba, Tsukuba, Japan

and

H.L. TANAKA

Institute of Geoscience, University of Tsukuba, Tsukuba, Japan
Frontier Research System for Global Change, International Arctic Research Center

(Manuscript received 24 April 2001, in revised form 30 January 2002)

Journal of the Meteorological Society of Japan
Vol. 80, No. 3
Meteorological Society of Japan

Journal of the Meteorological Society of Japan, Vol. 80, No. 3, pp. 387–402, 2002

Characteristics of Barotropic-Baroclinic Interactions during the Formation of Blocking Events in the Pacific Region

Yasushi WATARAI

Doctoral Program in Geoscience, University of Tsukuba, Tsukuba, Japan

and

H.L. TANAKA

Institute of Geoscience, University of Tsukuba, Tsukuba, Japan
Frontier Research System for Global Change, International Arctic Research Center

(Manuscript received 24 April 2001, in revised form 30 January 2002)

Abstract

In this study, characteristics of barotropic-baroclinic conversions of kinetic energy $C(K_s, K_m)$ are examined for atmospheric blocking, using the NCEP/NCAR reanalysis data. The energetics analysis was based on the formula derived originally by Wiin-Nielsen (1962).

As a result of case studies and composite analysis, we found that there were two maxima of $C(K_s, K_m)$ located along the western and eastern flanks of the blocking ridge, indicating that the baroclinic kinetic energy is converted to the barotropic kinetic energy in those regions. On the other hand, for a non-blocking case, where a ridge had amplified rapidly but not evolved into the blocking, the interactions $C(K_s, K_m)$ indicate only one maximum along the western flank of the ridge.

Around the blocking region, the nondivergent part of $C(K_s, K_m)$ was a large contributor, which is associated with temperature advection. As a meridional flow is further amplified, the enhanced temperature advection associated with the meridional flow induces larger conversion of $C(K_s, K_m)$. Because a blocking flow is characterized by an amplified meridional flow, especially for the barotropic component, the barotropic-baroclinic interactions $C(K_s, K_m)$ appear to play an important role for the formation of a blocking.

1. Introduction

The speculation that an atmospheric blocking is induced by traveling synoptic disturbances was proposed by meteorologists in the 1950s (e.g., Berggren et al. 1949; Rex 1950). In the late 1970s, Green (1977) discussed dynamical interpretation of this problem related to the European blocking of July 1976. Shutts (1983) demonstrated, using a barotropic model, that a basic flow with a dipole blocking pattern is maintained by the vorticity advection due to traveling eddies. The concept of the eddy forcing by synoptic disturbances for a blocking, i.e., an eddy straining hypothesis, is a likely candidate for the theory of blocking onset and maintenance, and is supported by many studies in recent years (e.g., Hansen and Sutera 1984; Mullen 1987; Haines and Marshall 1987; Nakamura and Wallace 1990; Tanaka 1991, 1998; Marques and Rao 1999).

It is known that a blocking has an equivalent-barotropic structure. Also, the life-

Corresponding author and present affiliation: Hiroshi L. Tanaka, Institute of Geoscience, University of Tsukuba, 1-1-1 Tennoudai, Tsukuba 305-8571, Japan.
E-mail: tanaka@atm.geo.tsukuba.ac.jp

cycle of a baroclinic wave, simulated by Simmons and Hoskins (1978) for the first time, indicates that the structure became barotropic for its decaying period. It may be possible that the constructive effect of eddies for a blocking is explained within the framework of the barotropic dynamics. Many blocking studies, such as Shutts (1983), Haines and Marshall (1987), and others, employed barotropic models.

On the other hand, many studies suggested that the baroclinic process plays a significant role as well, especially during the period of block formation. Colucci (1985) examined the case of explosive cyclone with a downstream blocking anticyclone. He showed that the blocking was forced by both thermal and vorticity advections. The same result was given by Alberta et al. (1991). Tsou and Smith (1990) examined height tendencies during the development of a blocking event. They indicated that the temperature advection indirectly influenced the blocking formation through the synoptic and synoptic-planetary interaction, although the direct forcing by the temperature advection was much weaker than that by the vorticity advection. Using a diagnostic method, Lupo (1997), and Lupo and Smith (1998), also found that the temperature advection was important during the formation of some blockings. Using a simple barotropic model with a realistic wavemaker, Tanaka (1998) demonstrated that the onset of blocking is led by a Rossby wave breaking, which is forced by barotropic-baroclinic interactions.

Tanaka and Kung (1988) showed, as a result of the three-dimensional normal mode energetics during the FGGE period, that the conversion from synoptic-scale baroclinic energy to planetary-scale barotropic energy occurred as a precursor of blocking. This implies the occurrence of barotropic-baroclinic interactions in the blocking formation. Several studies demonstrated that the Pacific and the Atlantic blockings appear independent of each other, so that the blocking is a local phenomenon, from a statistical (Lejenäs and Økland 1983), or a dynamical (Lupo 1997), viewpoint. Therefore, global spectral energetics like Tanaka and Kung (1988) may not represent the characteristics associated with pure blocking activities.

Kinetic energy conversions between the barotropic and baroclinic components have been studied since the beginning of 1960s. Wiin-Nielsen (1962) first proposed a set of kinetic energy equations divided in the vertical mean (barotropic) and shear (baroclinic) components. He evaluated the conversion term between these two components from observed data in January 1959 and found that the conversions have a maximum around zonal wave number 7 of synoptic eddies. Chen (1983) computed the same term for the tropics in the FGGE summer.

Wiin-Nielsen (1962) carried out the evaluations in the zonal spectral domain, and the results were averaged over the Northern Hemisphere. From a local point of view, some studies have been carried out using a formulation analogous to Wiin-Nielsen's (1962). Alpert (1981) investigated the local energetics for two cyclones over North America. Here, a kinetic energy budget was computed over the domain covering a cyclone. Chen and Yen (1985) showed the horizontal distribution of each term of the kinetic energy equations in the Northern Hemisphere and examined the local maintenance of the barotropic and baroclinic kinetic energies for two models and for observation. Thus, many of the studies using the barotropic and baroclinic kinetic energy equations have presented a long-term mean, or cases of extratropical cyclones. Yet, there have been few studies of the local energetics dealing with an atmospheric blocking using the barotropic-baroclinic decomposition.

The purpose of this study is to investigate the characteristics of the energy conversion from baroclinic to barotropic components associated with the blocking, based on a local energetics. In order to accomplish this task, we use barotropic and baroclinic kinetic energy equations derived by Wiin-Nielsen (1962) and extended by Chen and Yen (1985).

A blocking phenomenon has characteristic spatial and temporal structures. By using such a particularity, a number of studies of the local energetics distinguishes the blocking from other phenomena. For example, Mak (1991) identified the blocking as the intraseasonal component of temporal decomposition. He divided the field variables into three components (seasonal, intraseasonal and high-frequency) and examined the role of interactions among these components in the formation and main-

tenance of a blocking event. Lupo (1997) considered the horizontal scale of phenomena and partitioned the fields into two components (planetary- and synoptic-scales). On the other hand, we introduce the vertical scale decomposition as mentioned above. Correctly, a blocking pattern has both barotropic and baroclinic components since it is not a perfect barotropic structure, but equivalent-barotropic. The barotropic-baroclinic interactions in the blocking region, therefore, include not only the interaction with eddies of synoptic- and planetary-scales, but the self-interaction of the blocking. However, we expect that the essence of blocking structure is barotropic and that the barotropic-baroclinic interactions around the blocking ridge are dominated by the interactions with baroclinic synoptic eddies. We are interested in the behavior of barotropic-baroclinic interactions during the formation of blocking phenomena, and it seems that more study is required.

We present the data and the analysis methods of this study in Section 2. The results of a typical Pacific blocking case in February 1989 and a nonblocking case in January 1989 are shown in Section 3. The composite analysis for 10 blocking events in the Pacific is examined in Section 4. Discussion and conclusions are in Sections 5 and 6, respectively.

2. Data and analysis method

2.1 Data

The data used in this study are four-time-daily (0000, 0600, 1200 and 1800 UTC) reanalysis provided by the National Center for Environmental Prediction (NCEP) (see Kalnay et al. 1996). The variables provided by the data set are horizontal wind, $\mathbf{V} = (u, v)$, and geopotential height, $z = \phi/g$, where ϕ is geopotential, for 20 winters (November to March) from 1978/79 to 1997/98. The horizontal grid interval of the data is 2.5° × 2.5°, and the vertical grids are defined at 17 pressure levels at 1000, 925, 850, 700, 600, 500, 400, 300, 250, 200, 150, 100, 70, 50, 30, 20 and 10 hPa.

2.2 Kinetic energy equations for the barotropic and baroclinic components

In this study, we focus on the local kinetic energy conversions between the barotropic and baroclinic flows, which are called "barotropic-baroclinic interactions" in this paper, during the formation of the blocking. To examine these interactions, it is necessary to use the kinetic energy equations separated into the two flow components. Wiin-Nielsen (1962) formulated global mean kinetic energy equations of the vertical mean and shear (deviation from the vertical mean) components. Chen and Yen (1985) extended Wiin-Nielsen's formula so that they could deal with the energies locally. They examined the winter-mean distributions of the barotropic-baroclinic interactions and other terms in the Northern Hemisphere, using the ECMWF FGGE III-b analysis data extended from December 1978 to February 1979. Therefore, according to their antecedent papers, we compute the barotropic-baroclinic interactions on the basis of the kinetic energy equations of the barotropic and baroclinic components.

For each meteorological variable, $\xi = u, v$ or ϕ, the barotropic (i.e., the vertical mean) and baroclinic (the vertical shear) operators are defined by the following:

$$\xi_m = \frac{1}{p_s}\int_0^{p_s} \xi \, dp, \tag{1}$$

$$\xi_s = \xi - \xi_m, \tag{2}$$

where p_s is the surface pressure, and subscript m and s represent the barotropic and baroclinic components, respectively.

The kinetic energies of the barotropic and baroclinic components are

$$k_m = \frac{u_m^2 + v_m^2}{2}, \tag{3}$$

$$k_s = \frac{u_s^2 + v_s^2}{2}, \tag{4}$$

respectively. The total (the sum of barotropic and baroclinic) kinetic energy is then written

$$k = k_m + k_s + \mathbf{V}_m \cdot \mathbf{V}_s. \tag{5}$$

The inner-product term, $\mathbf{V}_m \cdot \mathbf{V}_s$, can be eliminated when mass-integrated vertically from the top to bottom of the atmosphere since $(( )_s)_m = 0$, and then

$$K = \frac{p_s}{g} k_m + \frac{p_s}{g} (k_s)_m,$$
$$= K_m + K_s, \tag{6}$$

where the vertically mass-integrated kinetic energy variables are designated by capital K.

The vertically-integrated prognostic equations of the barotropic and baroclinic kinetic energies are given in the pressure coordinate over the sphere by

$$\frac{\partial K_m}{\partial t} = -\frac{p_s}{g}(\nabla \cdot k\mathbf{V}_m)_m - \frac{p_s}{g}\mathbf{V}_m \cdot \nabla\phi_m - \frac{p_s}{g}\{\mathbf{V}_m \cdot (\mathbf{k}\times\mathbf{V}_s)\zeta_s\}_m - \frac{p_s}{g}\{(\mathbf{V}_m \cdot \mathbf{V}_s)\nabla \cdot \mathbf{V}_s\}_m + \frac{p_s}{g}\mathbf{V}_m \cdot \mathbf{F}_m, \quad (7)$$

$$\frac{\partial K_s}{\partial t} = -\frac{p_s}{g}(\nabla \cdot k\mathbf{V}_s)_m - \frac{p_s}{g}(\mathbf{V}_s \cdot \nabla\phi_s)_m + \frac{p_s}{g}\{\mathbf{V}_m \cdot (\mathbf{k}\times\mathbf{V}_s)\zeta_s\}_m + \frac{p_s}{g}\{(\mathbf{V}_m \cdot \mathbf{V}_s)\nabla \cdot \mathbf{V}_s\}_m + \frac{p_s}{g}(\mathbf{V}_s \cdot \mathbf{F}_s)_m, \quad (8)$$

where $\mathbf{k}$ is a unit vector of vertical direction, $\zeta = \mathbf{k} \cdot (\nabla \times \mathbf{V})$ is the vertical component of relative vorticity, and $\mathbf{F}$ is a frictional forcing vector. Here we have assumed that $\omega = 0$ at the top and bottom of the atmosphere as the boundary condition.

On the right-hand side of (7), the first term is the convergence of kinetic energy flux by barotropic flow and is represented by $B(K_m)$ hereafter. The second term is the generation of barotropic kinetic energy by barotropic ageostrophic flow $G(K_m)$. The fifth term is the frictional dissipation for barotropic kinetic energy $D(K_m)$. Similarly, on the right-hand side of (8), the first, second, and fifth terms are the convergence of kinetic energy flux by baroclinic flow $B(K_s)$, the generation of baroclinic kinetic energy $G(K_s)$, and the dissipation for baroclinic kinetic energy $D(K_s)$, respectively.

Equations (7) and (8) have an equivalent magnitude but opposite sign for the third and fourth term of the right-hand side, and then they represent the conversion between the barotropic and baroclinic flow, i.e., barotropic-baroclinic interactions, $C(K_s,K_m)$. It is usually positive on the average of a large area. For example, Chen and Yen (1985) estimated the mean value of $C(K_s,K_m)$ over the Northern Hemisphere for a winter (December 1978 to February 1979) using the ECMWF data and obtained a value of 1.33 Wm^{-2}. According to our estimate, using the NCEP/NCAR reanalysis, a similar value of 1.40 Wm^{-2} is obtained for December 1988 to February 1989. Examining the barotropic-baroclinic interaction term in more detail, it is clear that it consists of two parts, nondivergent (C_{ND}) and divergent (C_D):

$$C_{ND}(K_s,K_m) = -\frac{p_s}{g}\{\mathbf{V}_m \cdot (\mathbf{k}\times\mathbf{V}_s)\zeta_s\}_m, \quad (9)$$

$$C_D(K_s,K_m) = -\frac{p_s}{g}\{(\mathbf{V}_m \cdot \mathbf{V}_s)\nabla \cdot \mathbf{V}_s\}_m. \quad (10)$$

Finally, (7) and (8) can be rewritten as

$$\frac{\partial K_m}{\partial t} = B(K_m) + G(K_m) + C(K_s,K_m) - D(K_m), \quad (11)$$

$$\frac{\partial K_s}{\partial t} = B(K_s) + G(K_s) - C(K_s,K_m) - D(K_s), \quad (12)$$

and is illustrated with an energy box diagram, as shown in Fig. 1.

2.3 *Vertical normal mode expansion*

Kasahara and Puri (1981) described the spectral expansion scheme with 3-dimensional normal mode functions (3-D NMFs). The 3-D NMFs are orthonormal functions consisting of the Hough harmonics, which are bases of the horizontal directions, and the vertical structure functions as a base of the vertical direction. Using the 3-D NMFs, there are several studies

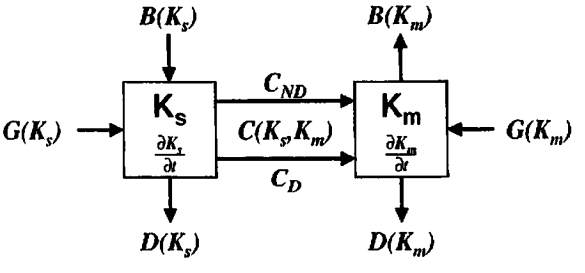

Fig. 1. The energy box diagram for barotropic and baroclinic kinetic energies. Refer to the text for the definition of variables. Arrows point out the direction of the kinetic energy conversion for a typical baroclinic cyclone (Cyclone II) examined by Alpert (1981).

of global energetics published in which estimates of the energy conversions between any pair of 3-dimensional spatial scale components are made (Tanaka 1985; Tanaka and Kung 1988, 1989).

A separation of variables is applied to the set of linearized primitive equations. As a result, the vertical structure equation is given by

$$\frac{\partial}{\partial\sigma}\frac{\sigma^2}{R\gamma}\frac{\partial G_n(\sigma)}{\partial\sigma}+\frac{1}{gh_n}G_n(\sigma)=0, \tag{13}$$

where $\sigma = p/p_s$, subscript n is the vertical mode number, and h_n is an equivalent depth. The symbol $\gamma = (RT_0/c_p) - (dT_0/d\ln\sigma)$ is a static stability parameter, where T_0 is the global mean temperature depending on pressure, R the gas constant for dry air, and c_p the specific heat at constant pressure. The vertical structure (normal mode) functions, $G_n(\sigma)$, can be obtained as the eigenfunctions of equation (13).

The vertical normal mode functions satisfy the orthonormal condition, then we can perform the following vertical transforms:

$$f(\sigma)=\sum_{n=0}^{\infty}f_nG_n(\sigma), \tag{14}$$

$$f_n=\int_0^1 f(\sigma)G_n(\sigma)\,d\sigma, \tag{15}$$

where f is an arbitrary function depending on σ. Therefore, (14) and (15) can be used to partition the flow and mass fields into their barotropic and baroclinic components.

In this study, the vertical modes are truncated from $n = 0$ to 11, and as an approximation, expression (1) is replaced by the $n = 0$ component (the barotropic mode), while (2) is replaced by the sum of the $n = 1$ to 11 components (the baroclinic mode). In fact, we verify that the barotropic-baroclinic decomposition estimated by the vertical normal mode expansion (14) and (15) is approximately same as the original definition of each term in (11) and (12) (figure not shown).

2.4 *Definition of blocking*

To identify a blocking event as objectively as possible, we have employed Mullen's (1987) blocking index. The Mullen index defines a blocking event as the ridge when the mean 500 hPa geopotential height over the 50–60°N belt along a certain longitudinal line is 150 m higher than the average of the nearby 90° longitude sector. Here, the 500 hPa geopotential height is low-pass filtered using the Blackmon et al. (1986) procedure before blocking events are selected. Mullen index with Blackmon filter is evaluated by using only twice daily data at 0000 and 1200 UTC.

In order to select more typical and fewer blocking events, we utilize Lejenäs and Øklands' (1983) index as an another subsidiary restriction in addition to the Mullen index. Here, Lejenäs and Økland index is defined as the 500 hPa geopotential height difference between 40°N and 60°N along a certain longitudinal line. In performing the composite analysis, these two indices for blocking events are superimposed in Hovmöller diagram (e.g., Fig. 2). Blocking events are identified in this study when these two indices satisfy those blocking criteria.

We define the onset of blocking events by the time when Mullen index first exceeds the threshold value of 150 m. The mature stage is defined by the time when Mullen index reaches its maximum. In this study, since we have shown a blocking occurred over Alaska, we analyze only the Pacific blocking that formed along the 150°W meridian. A list of the 10 selected blocking events and their onset and mature time is shown in Table 1.

3. Case studies

3.1 *Case study of a Pacific blocking: February 1989*

In this subsection, we examined a Pacific Region blocking event that occurred in late January, 1989. This blocking had a typical "Ω"-like pattern, and persisted for nearly a month. In the Alaskan region, where the center of the blocking anticyclone was located, surface air temperatures warmed unusually, as much as 40 K a week (e.g., Tanaka and Milkovich 1990).

Figure 3 shows the horizontal distributions of 5-day mean 500 hPa geopotential height before and after the formation of blocking in the Pacific region. The midlatitude mass field over the North Pacific ocean represents the predominant zonal geostrophic flow before and around 20 January, prior to the onset of blocking (Fig. 3a). In late January, the midlatitude flow began to meander and a double-jet structure arose near

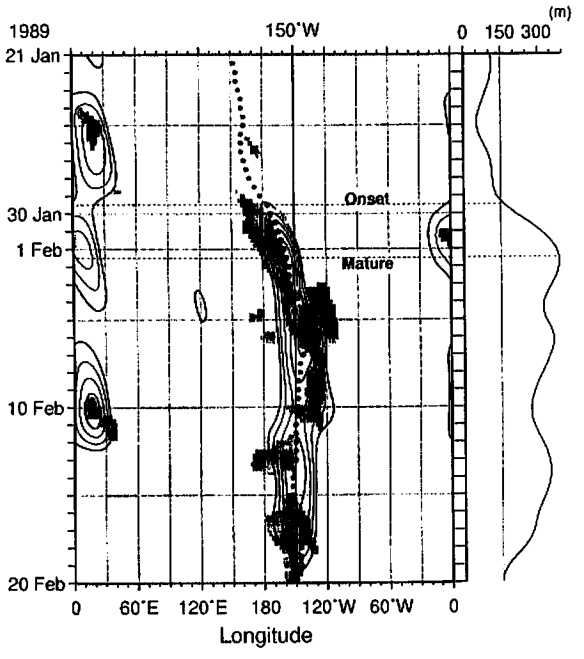

Fig. 2. An example of a Pacific (Alaskan) blocking taken by two blocking indices (on February 1989, No. 5 in Table 1): The solid line with a 50 m interval shows the magnitude of Mullen's (1987) index, which is illustrated for more than 150 m (i.e., the threshold value). The shaded area shows the negative value of Lejenäs and Øklands' (1983) index. The thick dotted line shows the maximum of Mullen index at any instant through the notable blocking. The right panel illustrates the magnitude of Mullen index along the thick dotted line.

Table 1. A list of the Pacific (Alaskan) blockings taken by using both Mullen's (1987) and Lejenäs and Øklands' (1983) indices.

No.	Onset Time				Mature Time			
1	12Z	2	January	1979	00Z	5	January	1979
2	12Z	31	January	1982	00Z	7	February	1982
3	00Z	15	December	1983	00Z	23	December	1983
4	00Z	28	December	1987	00Z	2	January	1988
5	12Z	29	January	1989	12Z	1	February	1989
6	00Z	19	January	1991	12Z	25	January	1991
7	00Z	23	February	1991	00Z	26	February	1991
8	00Z	13	February	1993	12Z	17	February	1993
9	00Z	28	January	1994	00Z	1	February	1994
10	12Z	24	February	1996	00Z	1	March	1996

180° longitude (Fig. 3b). The ridge formed rapidly and developed as it slowly moved eastward. At the same time, another ridge over the west coast of North America developed and retrograded. At last, these two ridges merged, and intense Ω-type blocking formed, showing the anticyclonic center over the Alaskan region (Fig. 3c). The blocking high stayed at this region and maintained its strength, moving slightly southeastward and expanding its size (Fig. 3d). Thereafter, this blocking was maintained until the beginning of March, with some intermissions (not shown).

Figure 4 shows the distributions of barotropic-baroclinic interactions, $C(K_s,K_m)$, for each 5-day mean period. First, $C(K_s,K_m)$ has positive value over wide areas of the Northern Hemisphere for each period. Second, we note that there is a quasi-stationary maximum of $C(K_s,K_m)$ over the area from Japan to 180° longitude along the midlatitude jet stream. It corresponds to the region of the so-called stormtrack where synoptic eddies are most active.

As the blocking ridge grows over the Bering Sea, the maxima of $C(K_s,K_m)$ locate along both western and eastern flanks of the ridge (Fig. 4b). It seems that such a pair of maxima is maintained and slightly intensified during the formation of blocking. In Fig. 4c, which corresponds to the mature time of the blocking (see Fig. 2 and Table 1), those values become about 30 Wm^{-2} and are comparable to the maximum along the stormtrack region. Afterwards, the pair of maxima remained as shown by Fig. 4(d), although the western maximum grew a little and the eastern decayed.

As discussed in Section 2.2, the barotropic-baroclinic interactions $C(K_s,K_m)$ are divided into the nondivergent part $C_{ND}(K_s,K_m)$ and divergent part $C_D(K_s,K_m)$ as expressed by (9) and (10), respectively. When we divide the term $C(K_s,K_m)$ into these two components, it is found that the term $C_{ND}(K_s,K_m)$ dominates in every period, especially around the blocking region. Although the term $C_D(K_s,K_m)$ is comparable to $C_{ND}(K_s,K_m)$ over the stormtrack region for 5-day mean field, the contribution of $C_D(K_s,K_m)$ becomes small near the blocking region (figure not shown).

Figure 5 shows a mean energy box diagram for 31 January to 4 February. Each energy and energy conversion in the diagram is averaged

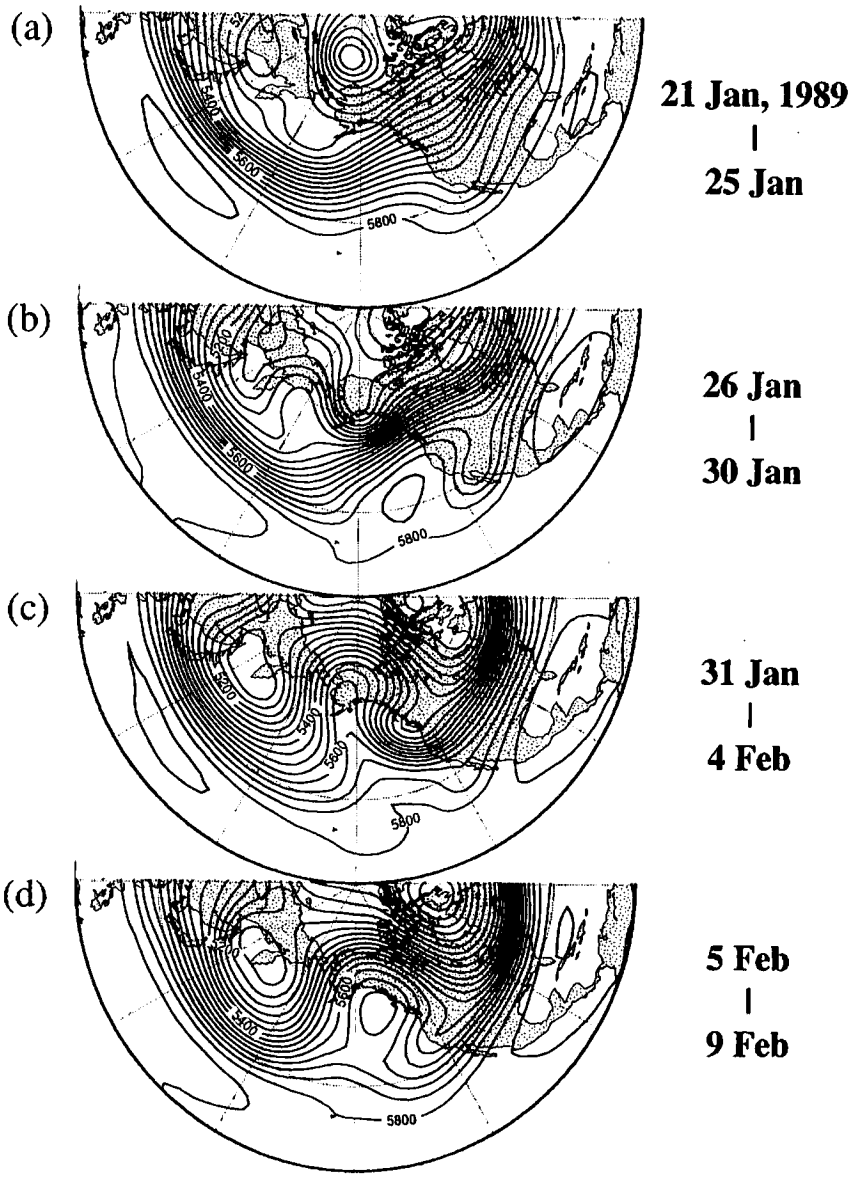

Fig. 3. 5-day mean fields of 500 hPa geopotential height in the formation of the Pacific blocking from the late of January to the beginning of February, 1989. Contour interval is 50 m.

over the area of 30°N to 80°N and 165°E to 105°W.

When the blocking ridge is developing most rapidly (Fig. 5), baroclinic kinetic energy K_s is principally supplied by $G(K_s)$. The flux contribution $B(K_s)$ is only one third of $G(K_s)$. Then, K_s is extracted by $D(K_s)$ and $C(K_s,K_m)$. Contribution of $C(K_s,K_m)$ is comparable to that of $D(K_s)$. While $C_D(K_s,K_m)$ contributes the increase of K_s, $C_{ND}(K_s,K_m)$ converts K_s to K_m. Since the magnitude of $C_{ND}(K_s,K_m)$ is much larger than that of $C_D(K_s,K_m)$, $C(K_s,K_m)$ totally converts K_s to K_m. K_m is supplied by $B(K_m)$ and $C(K_s,K_m)$, which have nearly equal contributions. Finally, K_m is mainly dissipated by $D(K_m)$.

3.2 *Case study of a nonblocking: January 1989*

In order to understand energy flows during the blocking discussed in the previous subsection, we compare the blocking case with a non-

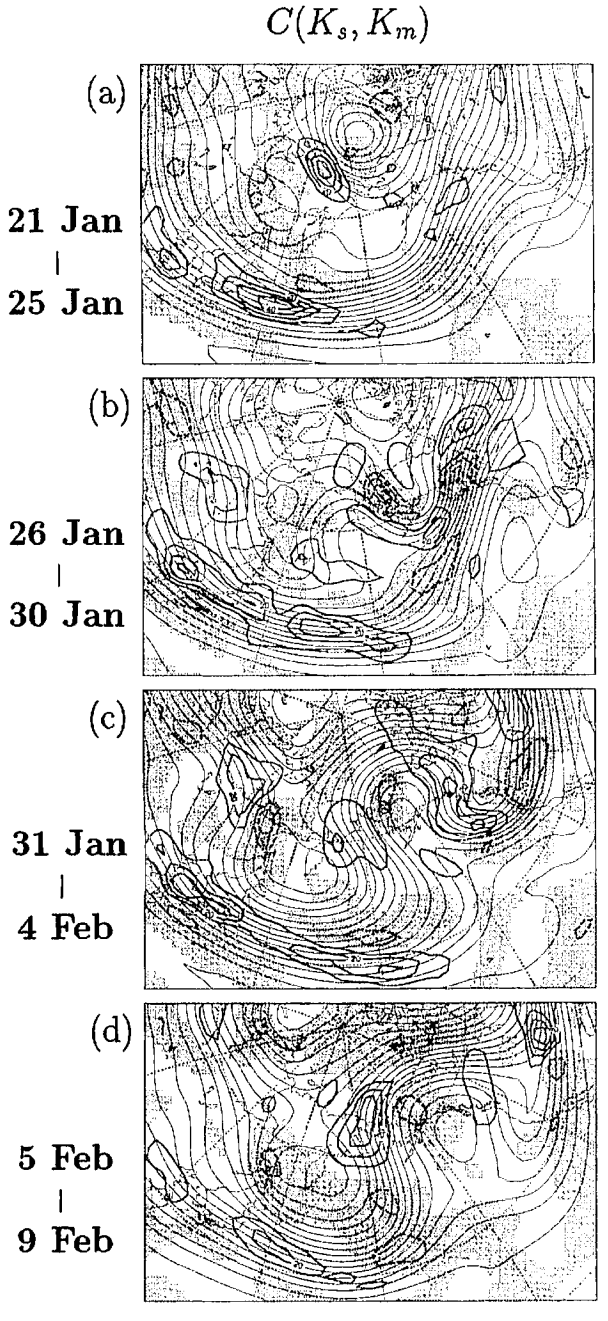

Fig. 4. Distributions of 5-day mean barotropic-baroclinic interaction term, $C(K_s, K_m)$, for the same periods as Fig. 3 (thick solid lines), where negative values are illustrated by dashed contours and shaded areas. Contour interval is 10 Wm^{-2}. Thin solid lines show 5-day mean 500 hPa geopotential height as in Fig. 3.

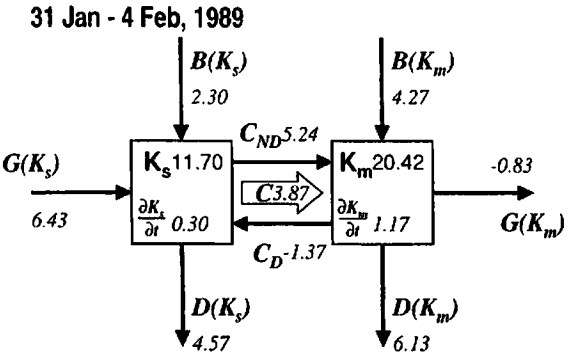

Fig. 5. The blocking area (165°E–105°W, 30–80°N) mean energy box diagram with regard to the same period of Fig. 3(c). Units are 10^5 Jm^{-2} for the kinetic energy variables (K_m and K_s) and Wm^{-2} for the kinetic energy changes.

blocking case in this subsection. In this study, we searched for a typical case in which a blocking was not formed, despite the sufficient amplification of a ridge. Such a case is found for the beginning of January 1989 over the Northeastern Pacific.

Figure 6 illustrates 5-day mean 500 hPa geopotential heights with regard to the nonblocking case. In the last few days of December 1988, a weak ridge moves eastward near 160°E and amplifies gradually in the daily weather charts along the jet axis over the Pacific (Fig. 6a). During the next five days from 3 to 7 January, the ridge amplifies rapidly, expands its meridional scale and then creates a pronounced ridge over Alaska, as seen in Fig. 6b. It appears to have larger amplitude extending to the North Pole. The ridge, however, moves eastward, reducing its amplitude without growing into a blocking event (Fig. 6c). At last, the flow becomes nearly zonal, as seen in Fig. 6d.

Figure 7 illustrates the distributions of the conversion term $C(K_s, K_m)$ for the nonblocking case. For the nonblocking ridge, we can find a notable maximum of $C(K_s, K_m)$ along the western flank of the ridge over the Bering Sea, as seen for the blocking case. The positive value is most intense when the ridge reaches the largest amplitude. The maximum is mostly contributed by $C_{ND}(K_s, K_m)$ (not shown). The maximum moves eastward, together with the ridge, and weakens. It is worthwhile to note

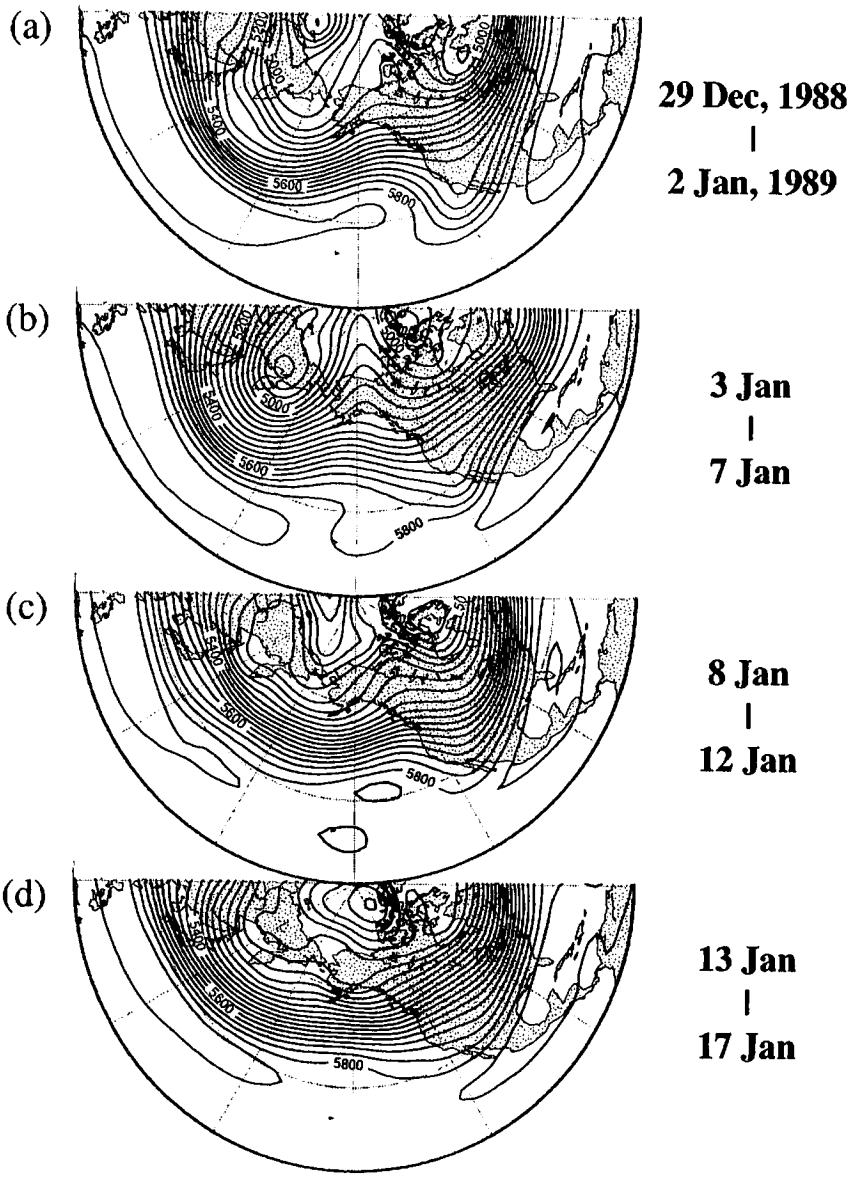

Fig. 6. As in Fig. 3, except for the nonblocking case at the beginning of January, 1989.

that the most interesting difference between the nonblocking case and the blocking case is the lack of another striking maximum along the eastern flank of the ridge. There is only one maximum of $C(K_s, K_m)$ located along the western flank of the ridge for the nonblocking case.

4. Composite analysis

In this section, we attempt to perform a composite analysis for blocking events selected from the long-term period of observed data. Blocking events are objectively defined as explained in Section 2.4. The compounded 10 blocking events in the Pacific region are shown in Table 1.

Before viewing the features of the barotropic-baroclinic interactions, we examine the distributions of barotropic and baroclinic kinetic energy fields. Figure 8 illustrates the composite distributions of (a) K_m and (b) K_s for the 10 blocking events during the 5-day mean around their mature time. Both K_m and K_s are large at the jet region around Japan. The maximum of K_m is located east of Japan, and its magnitude

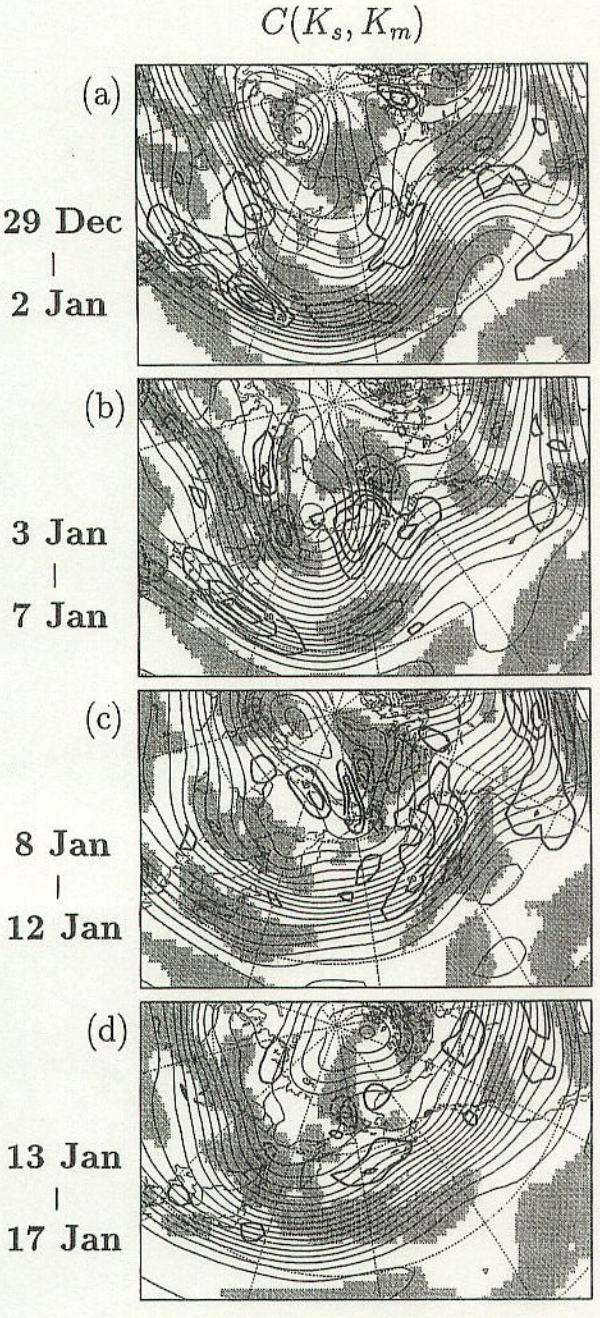

Fig. 7. As in Fig. 4, except for the non-blocking case.

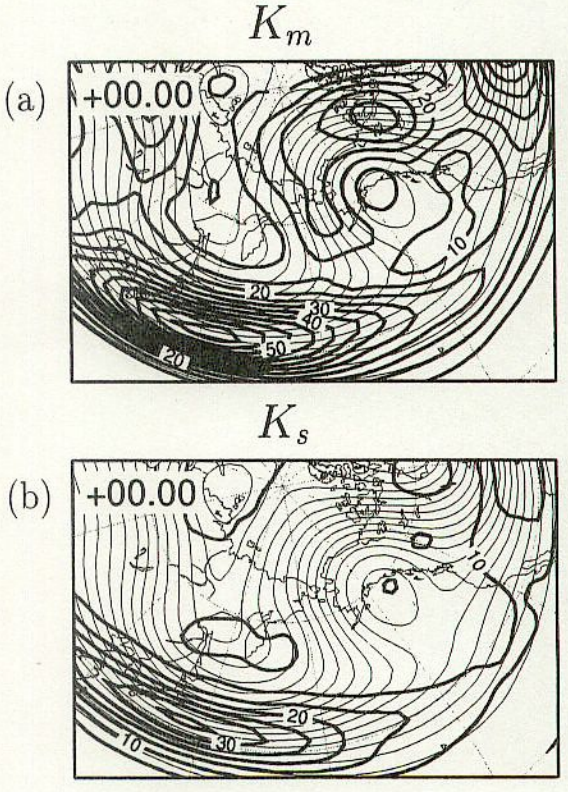

Fig. 8. Thick solid lines show distributions of 5-day mean (a) barotropic (K_m) and (b) baroclinic (K_s) components of kinetic energy for the mature time. Contour interval is 5×10^5 Jm^{-2}. Thin solid lines show 5-day mean 500 hPa geopotential height with 50 m interval.

is about 65×10^5 Jm^{-2}. The maximum of K_s is somewhat west, and the magnitude about half, of the maximum of K_m. In contrast, the jet around the blocking anticyclone indicates small K_s, suggesting that the flow is mostly barotropic. Both K_m and K_s are obviously small in the center of the blocking anticyclone, where winds are light.

Figures 9(a) to 9(e) show the composite distributions of a sequence of 5-day mean $C(K_s, K_m)$ centered at the mature time minus 4 day, minus 2 day, 0 day, plus 2 day, and plus 4 day, respectively, superimposed upon the composite 500 hPa geopotential height fields. Overall, the term $C(K_s, K_m)$ indicates a positive value at almost all the jet regions. A marked maximum is seen over Japan, as shown in Section 3.1. The position of the maximum lies further west of the maximum of K_s. At the equator side of the maximum, negative area of $C(K_s, K_m)$ (shaded area in Fig. 9) is seen, consistent with the result of seasonal mean field by Chen and Yen (1985). When we partition the term $C(K_s, K_m)$ in $C_{ND}(K_s, K_m)$ and $C_D(K_s, K_m)$, as shown by Fig. 10, we can find that $C_D(K_s, K_m)$ is comparable to $C_{ND}(K_s, K_m)$ over Japan. The term $C_{ND}(K_s, K_m)$ shows a dipole structure with

positive and negative regions divided by the 30°N line, while $C_D(K_s, K_m)$ indicates positive values over that area. Therefore, these two terms reinforce (offset) each other on the poleward (equatorward) side of the jet core.

For the blocking region in Fig. 9, there are two maxima of $C(K_s, K_m)$ along the western and eastern flanks of the blocking ridge, as is seen by the case study in Section 3.1. The pattern of two maxima is formed prior to the mature time, and slightly intensified as the blocking ridge amplifies (Figs. 9a, b). It seems that such a pattern appears with the onset of blockings (not shown). This pattern is most evident when the blockings reach their mature time (Fig. 9c). The peak value of the maxima is about 10 Wm^{-2}, which is as small as two-fifths of that over Japan. After the mature time, the maxima are weakened as the blockings decay (Figs. 9d, e). It is important to note that the two maxima in the blocking region mostly can be explained by the nondivergent part of $C(K_s, K_m)$ (Fig. 10a). In general, the divergent part of $C(K_s, K_m)$ is nearly zero or even negative in the blocking region (Fig. 10b).

The characteristics of the other energetics terms in (11) and (12) are briefly presented below. Figure 11 illustrates the composite distributions of the 5-day mean conversion of kinetic energy flux term (B) and generation (G). In general, we can see that B and G show similar distributions, but with opposite signs for both barotropic and baroclinic flows. This result is similar to those of Chen and Lee (1983). At the entrance of the jet, G is positive and B is negative, whereas the signs are opposite at the jet exit region. The magnitudes of B and G over the blocking region are rather small compared with the jet exit region.

The energy box diagram integrated over the blocking domain (165°E–105°W, 30–80°N) is shown for the mature time in Fig. 12. The features of the kinetic energy budget are similar to that in the former case study for February 1989, as shown in Fig. 5(a). The direction of the energy flow in the composite and the blocking case study are consistent. In Fig. 12, however, the energy supply for K_s by $G(K_s)$ is smaller, and the conversion $C(K_s, K_m)$ from K_s to K_m is also smaller. Therefore, contribution from $C(K_s, K_m)$ to K_m is about a half of $B(K_m)$ for the composite result.

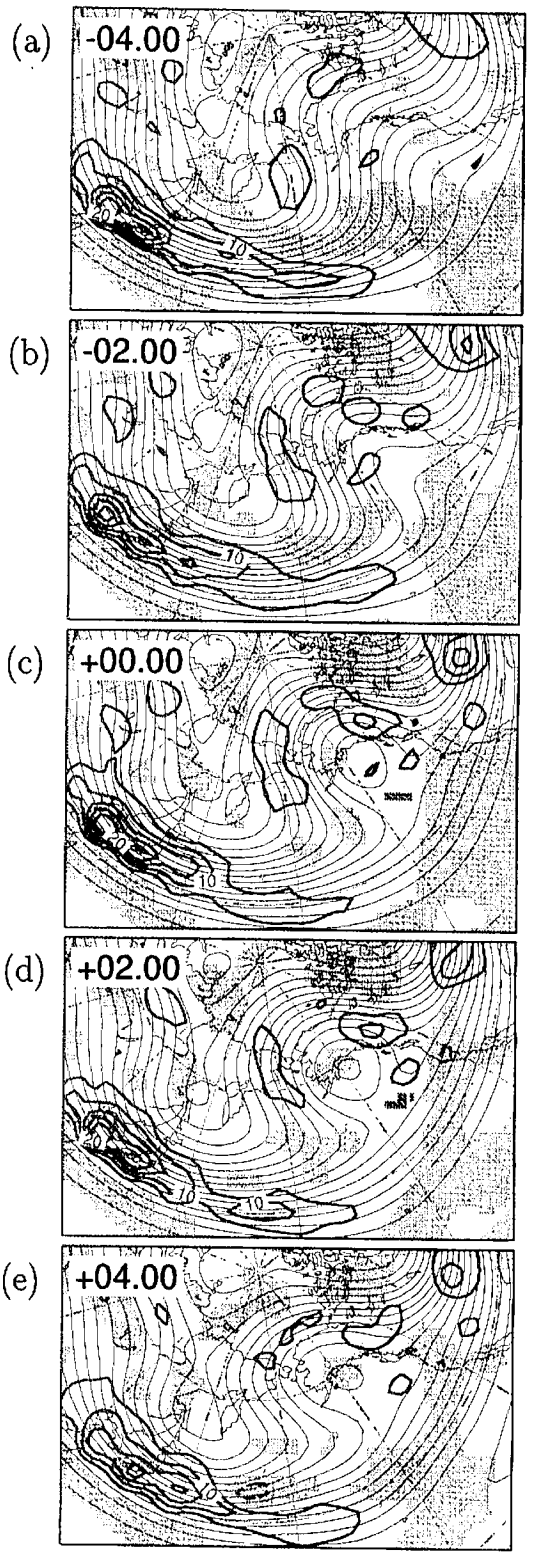

Fig. 9. As in Fig. 4, except for the Pacific blocking composite for −4, −2, 0, 2 and 4 day(s) relative to the mature time. Contour interval is 5 Wm^{-2}.

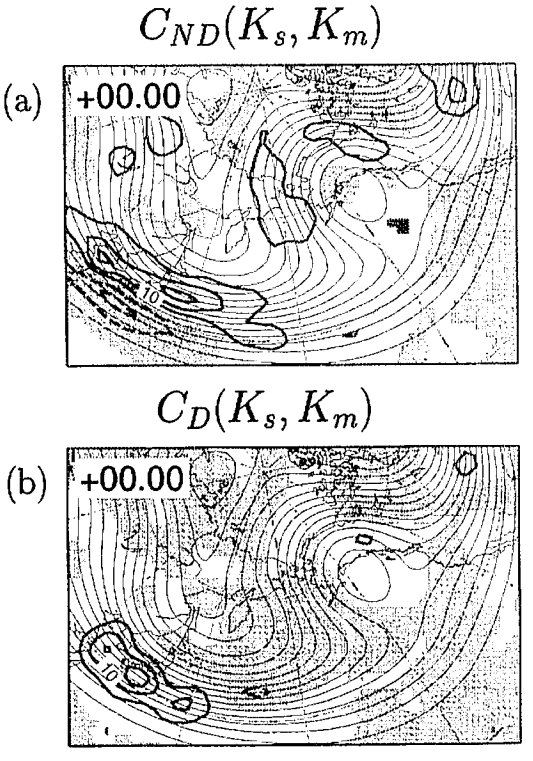

Fig. 10. Thick lines show distributions of 5-day mean (a) nondivergent (C_{ND}) and (b) divergent (C_D) parts of barotropic-baroclinic interaction term. Negative values are illustrated by dashed contours and shaded areas. Contour interval is 5 Wm^{-2}. Thin solid lines show 5-day mean 500 hPa geopotential height with 50 m interval.

5. Discussion

According to the case studies in Section 3, the maxima of $C(K_s,K_m)$ are analyzed along both western and eastern flanks of the ridge for the blocking case, whereas the maximum locates only along the western flank for the nonblocking case. Composite analysis for the blockings also shows the appearance of similar pattern. Therefore, we can suggest that the existence of the $C(K_s,K_m)$ maximum along the eastern flank of the ridge is the common feature in forming the blocking. In the nonblocking case, the developing ridge kept moving eastward and then decayed rapidly, whereas in the blocking case the ridge became quasi-stationary, staying at the same location for a long period. The maximum of $C(K_s,K_m)$ along the eastern flank of the ridge is the common feature when the blocking ridge becomes nearly stationary. On the other hand, for both cases, the maximum along the western flank of the ridge emerges when the ridge amplifies rapidly, and its magnitude becomes larger as ridge amplifies.

The vorticity forcing at the one-quarter wavelength upstream of the ridge, which was the common result of blockings and a nonblocking, was indicated by many studies (e.g., Illari 1984; Mullen 1987; Tsou and Smith 1990). Although the forcing mechanisms in these studies do not correspond directly to the barotropic-baroclinic interactions, it seems that their results are consistent with the results of this study, regarding the phase relationship. On the other hand, it seems that the maximum of $C(K_s,K_m)$ along the eastern flank of the ridge is an original finding. In the case of the Pacific blocking event of February 1989, we examined the evolution of $C(K_s,K_m)$ in more detail. The snapshots showed that the maxima of $C(K_s,K_m)$ moved corresponding to the traveling high-frequency eddies. It seems that the eastern maximum of $C(K_s,K_m)$ in the 5-day mean field resulted from the passage of high-frequency eddies (not shown), as in the case of the western maximum. In addition, the eastern maximum did not emerge for a nonblocking case. It may be that the occurrence of the eastern maximum is the key signal to distinguish whether the blocking is formed or not. The nonblocking case is, however, analyzed in this study only for one example. We therefore need to conduct a number of case studies or a composite analysis for many nonblocking cases to increase confidence in this study's findings. This is a topic for future work.

We now further discuss the features at the mature time by examining the other energetics terms for the composite fields of blocking cases (Fig. 11). We have shown that baroclinic kinetic energy K_s is generated by $G(K_s)$ at the entrance of the jet, then K_s is converted to K_m (positive $C(K_s,K_m)$). Meanwhile, barotropic kinetic energy K_m is also generated by $G(K_m)$ at the entrance of the jet near Japan, then K_m is transported eastward by $B(K_m)$ with westerly $\mathbf{V}_m$. The flux convergence of $B(K_m)$ has a noticeable maximum at the deformation field located along the western flank of the blocking, enhancing a great deal of K_m there.

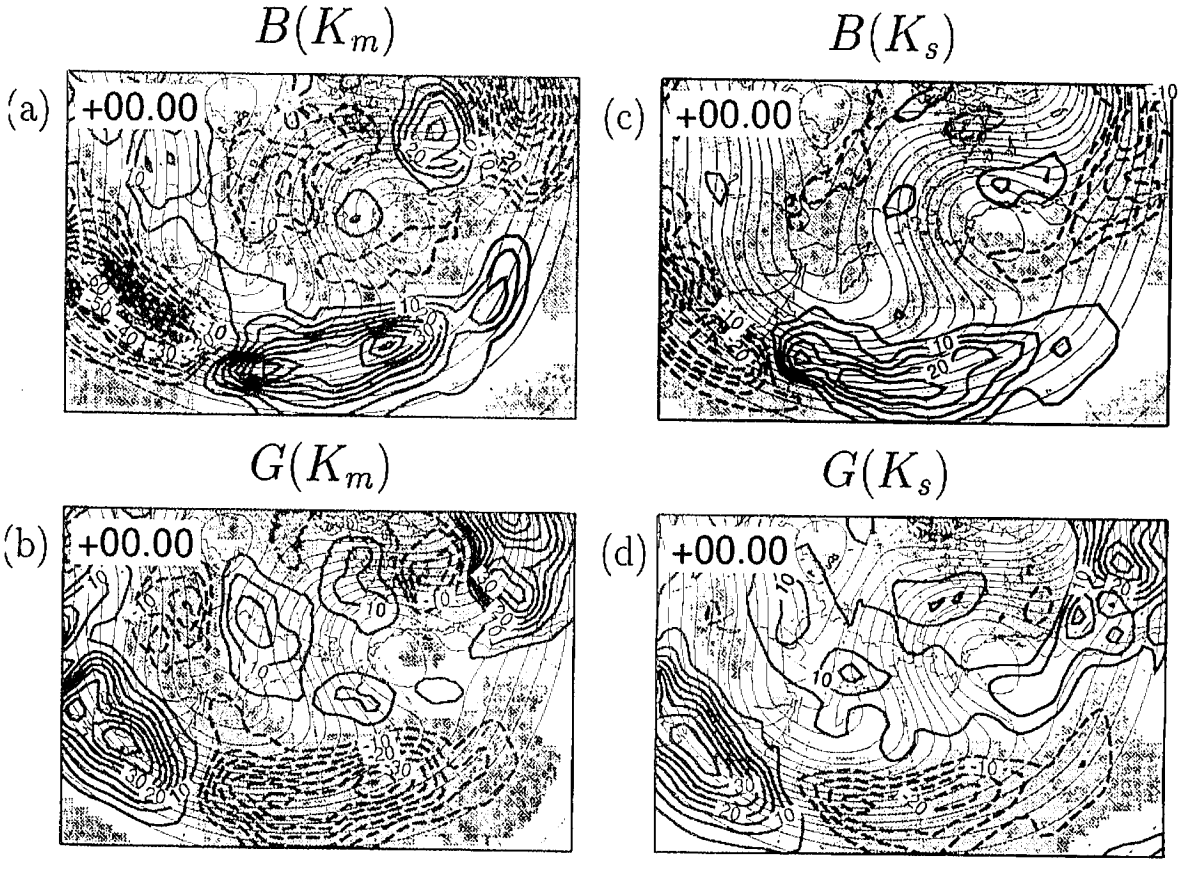

Fig. 11. Thick lines in each panel show distributions of 5-day mean fields with respect to convergence terms of kinetic energy flux (a, c) and generation terms (b, d) for the mature time. (a), (b) and (c), (d) are barotropic and baroclinic components, respectively. Negative values are illustrated by dashed contours and shaded areas. Contour interval is 5 Wm^{-2}. Thin solid lines show 5-day mean 500 hPa geopotential height with 50 m interval.

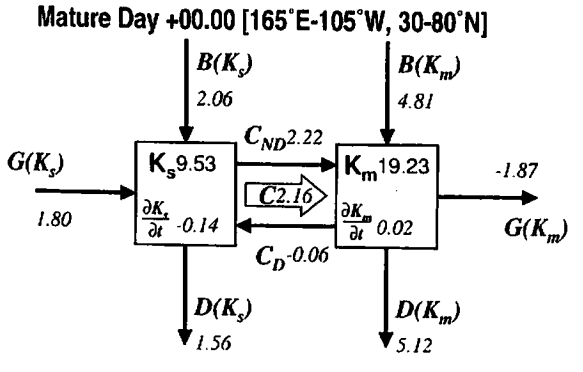

Fig. 12. As in Fig. 5, except for the Pacific blocking composite for the mature time.

As is mentioned above, $C(K_s, K_m)$ is divided in $C_{ND}(K_s, K_m)$ and $C_D(K_s, K_m)$. Assuming the flows are nondivergent, $C_{ND}(K_s, K_m)$ can be approximated as follows:

$$C_{ND}(K_s, K_m) \simeq -\{(\mathbf{V}_m \cdot \nabla\psi_s)\zeta_s\}_m. \quad (16)$$

If it is assumed that $\mathbf{V}_m$ is the flow in midtroposphere, $\psi_s = \psi - \psi_m$ is correspondent to the thermal streamfunction in upper atmosphere, and to the negative of the thermal streamfunction in lower atmosphere. The advection of thermal streamfunction is proportional to the temperature advection, $-\mathbf{V}_m \cdot \nabla T$. Therefore, $-\mathbf{V}_m \cdot \nabla\psi_s > 0$ expresses the warm (cold) air advection in lower (upper) atmosphere, and vice versa. ζ_s corresponds to the thermal vorticity in upper atmosphere and the opposite sign in lower atmosphere. It is then suggested that positive $C_{ND}(K_s, K_m)$ near Japan

corresponds to cold air advection behind the trough. On the other hand, according to Wiin-Nielsen and Chen (1993), $C_D(K_s,K_m)$ can be approximated as:

$$C_D(K_s,K_m) \simeq \{u_m u_s(-\nabla \cdot \mathbf{V}_s)\}_m, \qquad (17)$$

where for simplicity we have assumed that the zonal flow dominates. Equation (17) shows positive at downward wind and negative at upward wind along the midlatitude westerly jet. Therefore, the positive $C_D(K_s,K_m)$ near Japan corresponds to descending flow behind the trough.

Around the blocking ridge, positive G and negative B are dominant. Warm air surging poleward strengthens the temperature gradient around the blocking ridge. The large temperature gradient is one of the causes of positive $G(K_s)$ since it includes the conversion from available potential energy, as is discussed in Wiin-Nielsen and Chen (1993). A part of K_s generated by $G(K_s)$ will be immediately converted by $C(K_s,K_m)$. For each grid point, the term $C(K_s,K_m)$ is generally smaller than B or G. However, it becomes comparable for the average over the blocking area because it indicates positive value consistently within the area. Thus, $C(K_s,K_m)$ makes an important contribution to K_m, as well as $B(K_m)$, over the blocking area.

Here, $C(K_s,K_m)$ is mostly composed of $C_{ND}(K_s,K_m)$, associated with temperature advection. The maxima of $C(K_s,K_m)$ exist at the regions where the barotropic meridional flow is strong. Stronger meridional flow will likely lead to stronger temperature advection. Therefore, the two maxima of $C(K_s,K_m)$ are formed along both flanks of the blocking ridge. In more detail: in the area of western maximum, $-\mathbf{V}_m \cdot (\mathbf{k} \times \mathbf{V}_s)$, which corresponds to temperature advection, is positive and ζ_s is also positive in lower atmosphere, and both components are negative in upper atmosphere (figure not shown). It is therefore shown that there are strong warm air advections with anticyclonic thermal vorticity throughout most layers. This is consistent with the result of Colucci (1985). Contrarily, in the area of eastern maximum, both components are negative (positive) in lower (upper) atmosphere, and there are therefore strong cold air advections with cyclonic thermal vorticity. On the other hand, $C_D(K_s,K_m)$ is negative (positive) along the western (eastern) flank of the blocking ridge where upward (downward) motion dominates along with southerly (northerly) winds. Yet, the magnitude of this term is comparatively small.

Because a blocking flow is characterized by an amplified meridional flow, especially for the barotropic component, the increase of K_m located along the western and eastern flanks of the blocking ridge is the key factor for the formation of a blocking. According to the present analysis of a local energetics for K_m, the appearance of positive $C(K_s,K_m)$ along the key area is responsible for the increase of K_m. Hence, it is suggested that the barotropic-baroclinic interactions $C(K_s,K_m)$ along the western and eastern flanks of a ridge play an important role for the formation of a blocking.

6. Conclusion

In this study, we examined barotropic-baroclinic interactions for the atmospheric blocking, using the NCEP/NCAR reanalysis data. We employed the barotropic and the baroclinic kinetic energy equations as derived by Wiin-Nielsen (1962) and extended by Chen and Yen (1985). Special attention was given to the barotropic-baroclinic interactions $C(K_s,K_m)$ for kinetic energy. The analyses were performed and compared for a Pacific blocking case in February 1989 and for a nonblocking case in January 1989. We also conducted a composite analysis for 10 blockings selected objectively using definitions proposed by Mullen (1987) and Lejenäs and Økland (1983).

As a result, the overall energy flows associated with the blocking formation may be summarized as follows: The baroclinic kinetic energy K_s is principally supplied by $G(K_s)$. The flux contribution $B(K_s)$ is only one third as large as $G(K_s)$. Then, K_s is extracted by $D(K_s)$ and $C(K_s,K_m)$. Contribution of $C(K_s,K_m)$ is comparable to that of $D(K_s)$. While $C_D(K_s,K_m)$ contributes the increase of K_s, $C_{ND}(K_s,K_m)$ converts K_s to K_m. Since the magnitude of $C_{ND}(K_s,K_m)$ is much larger than that of $C_D(K_s,K_m)$, $C(K_s,K_m)$ as a whole converts K_s to K_m. K_m is supplied by $B(K_m)$ and $C(K_s,K_m)$. Finally, K_m is mainly dissipated by $D(K_m)$.

According to case studies, we found two maxima of barotropic-baroclinic interaction ($C(K_s,K_m)$) located along the western and east-

ern flanks of the blocking ridge, indicating that the baroclinic kinetic energy is converted to barotropic kinetic energy in those regions. On the other hand, for the nonblocking case, where a ridge had amplified rapidly but not evolved into the blocking, the interactions $C(K_s, K_m)$ indicate only one maximum along the western flank of the ridge.

The result from the composite analysis for 10 blocking cases has supported the conclusion derived from the case study. It is found that the appearance of two maxima of $C(K_s, K_m)$ along the western and eastern flanks of the blocking ridge is the common feature for many blockings. Around the blocking region, the term $C(K_s, K_m)$ is mostly contributed from the nondivergent part $(C_{ND}(K_s, K_m))$, which is associated with temperature advections. As a meridional flow is further amplified, the enhanced temperature advection associated with the meridional flow induces larger conversion of $C_{ND}(K_s, K_m)$. Because a blocking flow is characterized by an amplified meridional flow, especially for the barotropic component, the barotropic-baroclinic interactions $C(K_s, K_m)$ appear to play an important role for the formation of a blocking.

Finally, we should note that there is no need to expand the variables in the vertical normal modes for the barotropic-baroclinic decomposition in this study. The reason for it is a possible extension of the energetics toward the vertical spectral domain in various vertical scales. The study of such a vertical spectral energetics is, however, beyond the scope of this study, and we will reserve it for future work.

Acknowledgments

We thank Dr. T. Yasunari, Dr. F. Kimura, and graduate students in the climatology and meteorology group in the University of Tsukuba for a variety of advice and suggestions. We are also thankful to the reviewers for their helpful comments.

References

Alberta, T.L., S.J. Colucci and J.C. Davenport, 1991: Rapid 500-mb cyclogenesis and anticyclogenesis. *Mon. Wea. Rev.*, **119**, 1186–1204.

Alpert, J.C., 1981: An analysis of the kinetic energy budget for two extratropical cyclones: The vertically averaged flow and the vertical shear flow. *Mon. Wea. Rev.*, **109**, 1219–1232.

Berggren, R., B. Bolin and C.-G. Rossby, 1949: An aerological study of zonal motion, its perturbations and break-down. *Tellus*, **1**, 14–37.

Blackmon, M.L., S.L. Mullen and G.T. Bates, 1986: The climatology of blocking events in a perpetual January simulation of a spectral general circulation model. *J. Atmos. Sci.*, **43**, 1379–1405.

Chen, T.-C., 1983: The energy exchange between the baroclinic and barotropic components of atmospheric flow in the tropics during the FGGE summer. *Mon. Wea. Rev.*, **111**, 1389–1396.

——— and Y.-H. Lee, 1983: A study of the kinetic energy generation with general circulation models. *J. Meteor. Soc. Japan*, **61**, 439–448.

——— and M.-C. Yen, 1985: A note on the kinetic energy budget analysis of the atmospheric baroclinic and barotropic flows. *J. Meteor. Soc. Japan*, **63**, 685–693.

Colucci, S.J., 1985: Explosive cyclogenesis and large-scale circulation changes: Implications for atmospheric blocking. *J. Atmos. Sci.*, **42**, 2701–2717.

Green, J.S.A., 1977: The weather during July 1976: Some dynamical considerations of the drought. *Weather*, **32**, 120–126.

Haines, K. and J. Marshall, 1987: Eddy-forced coherent structures as a prototype of atmospheric blocking. *Quart. J. Roy. Meteor. Soc.*, **113**, 681–704.

Hansen, A.R. and A. Sutera, 1984: A comparison of the spectral energy and enstrophy budgets of blocking versus nonblocking periods. *Tellus*, **36A**, 52–63.

Kalnay, E., M. Kanamitsu, R. Kistler, W. Collins, D. Deaven, L. Gandin, M. Iredell, S. Saha, G. White, J. Woollen, Y. Zhu, M. Chelliah, W. Ebisuzaki, W. Higgins, J. Janowiak, K.C. Mo, C. Ropelewski, J. Wang, A. Leetmaa, R. Reynolds, R. Jenne and D. Joseph, 1996: The NCEP/NCAR 40-year reanalysis project. *Bull. Amer. Meteor. Soc.*, **77**, 437–471.

Kasahara, A. and K. Puri, 1981: Spectral representation of three-dimensional global data by expansion in normal mode functions. *Mon. Wea. Rev.*, **109**, 37–51.

Lejenäs, H. and H. Økland, 1983: Characteristics of northern hemisphere blocking as determined from a long time series of observational data. *Tellus*, **35A**, 350–362.

Lupo, A.R., 1997: A diagnosis of two blocking events that occurred simultaneously in the midlatitude northern hemisphere. *Mon. Wea. Rev.*, **125**, 1801–1823.

——— and P.J. Smith, 1998: The interactions between a midlatitude blocking anticyclone and synoptic-scale cyclones that occurred during

the summer season. *Mon. Wea. Rev.*, **126**, 502–515.

Mak, M., 1991: Dynamics of an atmospheric blocking as deduced from its local energetics. *Quart. J. Roy. Meteor. Soc.*, **117**, 477–493.

Marques, R.F.C. and V.B. Rao, 1999: A diagnosis of a long-lasting blocking event over the southeast Pacific ocean. *Mon. Wea. Rev.*, **127**, 1761–1776.

Mullen, S.L., 1987: Transient eddy forcing of blocking flows. *J. Atmos. Sci.*, **44**, 3–22.

Nakamura, H. and J.M. Wallace, 1990: Observed changes in baroclinic wave activity during the life cycles of low-frequency circulation anomalies. *J. Atmos. Sci.*, **47**, 1100–1116.

Rex, D.F., 1950: Blocking action in the middle troposphere and its effect upon regional climate I. an aerological study of blocking action. *Tellus*, **2**, 196–211.

Shutts, G.J., 1983: The propagation of eddies in diffluent jetstreams: eddy vorticity forcing of 'blocking' flow fields. *Quart. J. Roy. Meteor. Soc.*, **109**, 737–761.

Simmons, A.J. and B.J. Hoskins, 1978: The life cycles of some nonlinear baroclinic waves. *J. Atmos. Sci.*, **35**, 414–432.

Tanaka, H.L., 1985: Global energetics analysis by expansion into three-dimensional normal mode functions during the FGGE winter. *J. Meteor. Soc. Japan*, **63**, 180–200.

———, 1991: A numerical simulation of amplification of low-frequency planetary waves and blocking formations by the upscale energy cascade. *Mon. Wea. Rev.*, **119**, 2919–2935.

———, 1998: Numerical simulation of a life-cycle of atmospheric blocking and the analysis of potential vorticity using a simple barotropic model. *J. Meteor. Soc. Japan*, **76**, 983–1008.

——— and E.C. Kung, 1988: Nornal mode energetics of the general circulation during the FGGE year. *J. Atmos. Sci.*, **45**, 3723–3736.

——— and ———, 1989: A study of low-frequency unstable planetary waves in realistic zonal and zonally varying basic states. *Tellus*, **41A**, 179–199.

——— and M.F. Milkovich, 1990: A heat budget analysis of the polar troposphere in and around Alaska during the abnormal winter of 1988/89. *Mon. Wea. Rev.*, **118**, 1628–1639.

Tsou, C.-H. and P.J. Smith, 1990: The role of synoptic/planetary-scale interactions during the development of a blocking anticyclone. *Tellus*, **42A**, 174–193.

Wiin-Nielsen, A., 1962: On transformation of kinetic energy between the vertical shear flow and the vertical mean flow in the atmosphere. *Mon. Wea. Rev.*, **90**, 311–323.

——— and T.-C. Chen, 1993: *Fundamentals of Atmospheric Energetics*. Oxford University Press, 376pp.